JOURNAL OF CATALYSIS **162,** 54–65 (1996)
ARTICLE NO. 0259

A Comparative Study of CO and CO_2 Hydrogenation over Rh/SiO_2

Ian A. Fisher and Alexis T. Bell

Chemical Sciences Division, Lawrence Berkeley National Laboratory, Berkeley, California 94720; and Department of Chemical Engineering, University of California, Berkeley, California 94720

Received October 2, 1995; revised April 9, 1996; accepted April 10, 1996

The hydrogenation of CO and CO_2 over Rh/SiO_2 have been investigated for the purpose of identifying the similarities and differences between these two reaction systems. *In situ* infrared spectroscopy was used to characterize the surface of the catalyst. Exposure of the catalyst to CO or CO_2 produced very similar infrared spectra in which the principal features are those for linearly and bridge-bonded CO. In the case of CO_2 adsorption, a band for weakly adsorbed CO_2 could also be observed. For identical reaction conditions the rate of CO_2 hydrogenation to methane is higher than that for CO hydrogenation. The activation energy for CO hydrogenation is 23.2 kcal/mol and that for CO_2 hydrogenation is 16.6 kcal/mol. The partial pressure dependances on H_2 and CO_z (z = 1, 2) are 0.67 and −0.80, respectively, for CO hydrogenation, and 0.53 and −0.46, respectively, for CO_2 hydrogenation. Infrared spectroscopy reveals that under reaction conditions the catalyst surface is nearly saturated by adsorbed CO. The spectra observed during CO and CO_2 hydrogenation are similar, the principal difference being that the CO coverage during CO hydrogenation is somewhat higher than that during CO_2 hydrogenation. The CO coverage is insensitive to H_2 partial pressure, but increases slightly with increasing CO_z partial pressure. Transient-response experiments demonstrate that the adsorbed CO is a critical intermediate in both reaction systems. It is proposed that the rate determining step in the formation of methane is the dissociation of H_2CO, produced by the stepwise hydrogenation of adsorbed CO. A rate expression derived from the proposed mechanism properly describes the experimentally observed reaction kinetics both under steady-state and transient-response conditions.

INTRODUCTION

The hydrogenation of CO and CO_2 to form hydrocarbon and oxygenated products over supported and unsupported Rh has been the subject of extensive research. Numerous investigations have been reported for CO hydrogenation on polycrystalline Rh (1–6), and Rh supported on various oxide supports (7–34). CO_2 hydrogenation has also been investigated on polycrystalline Rh (1, 3–5, 35, 36) and supported Rh (26–28, 37–48). Comparison of the reported results for CO and CO_2 hydrogenation over polycrystalline Rh and SiO_2- or Al_2O_3-supported Rh reveals several significant differences: (1) The methane selectivity for CO_2 hydrogenation is near 100%, while that for CO hydrogenation is lower (∼90%). (2) The rate of methane formation is higher for CO_2 than for CO hydrogenation at similar reaction conditions [i.e., temperature and partial pressures of H_2 and CO_z ($z = 1, 2$)]. (3) The apparent activation energy for CO_2 methanation is lower than that for CO methanation under similar reaction conditions. While the mechanisms of CO and CO_2 methanation are thought to be similar, both involving the cleavage of the C–O bond in either adsorbed CO or a H_xCO species as the rate determining step, no attempt has been made to fully explain the differences noted above.

The present investigation was undertaken for the purpose of developing a deeper understanding of the similarities and differences between the synthesis of methane from CO and CO_2. To this end, we have investigated the interaction of CO and CO_2 with Rh/SiO_2 by *in situ* Fourier-transform infrared spectroscopy (FTIR). Both steady-state and transient response studies of CO and CO_2 hydrogenation were performed to determine the reaction kinetics and the effect of surface species concentrations on the catalytic rate of methane formation. These studies have led to new insights regarding the role of adsorbed CO on the rate of methane formation, and suggest that in both CO and CO_2 methanation the C–O bond cleavage occurs during the dissociation of adsorbed H_2CO, rather than during the direct dissociation of adsorbed CO.

EXPERIMENTAL

The Rh/SiO_2 catalyst was prepared by incipient wetness impregnation of amorphous silica (Cab-O-Sil M-5, 200 m^2/g) with an aqueous solution of $Rh(NO_3)_3$ (Alfa Products, 99.9%). The material was dried in a vacuum oven at 393 K for 4 h. Calcination was performed at 723 K for 3 h in 100 cm^3/min atmospheric pressure air. Prior to all experiments the catalyst was reduced at 548 K in 20 cm^3/min atmospheric pressure hydrogen for more than 5 h. The Rh content of the catalyst was found to be 3.4 ± 2.0 wt% Rh by X-ray fluorescence analysis. The average Rh particle size as determined by transmission electron microscopy (TEM) is 22 Å, corresponding to a Rh dispersion of 45%.

Matheson UHP H_2, CO, and Ar and Coleman instrument purity CO_2 were purified prior to use. Hydrogen was

0021-9717/96 $18.00

passed through a Deoxo unit (Engelhard) to remove O_2 impurities by forming water which is subsequently removed by a molecular sieve trap (3A Davidson grade 564). CO was passed through a bed of glass beads at 573 K to decompose iron carbonyls, followed by passage through an ascarite trap to remove CO_2 and a molecular sieve trap to remove water. Ar was passed through an oxysorb (CrO_3) trap to remove O_2 and then a molecular sieve trap to remove water. CO_2 was passed through a hopcalite trap (80% $MnO_2 + 20\%$ CuO) to remove CO and a molecular sieve trap to remove water.

In situ transmission infrared spectroscopy was performed with a 2 cm diameter catalyst disk of 0.2 mm thickness weighing 70 mg (22.3 mg/cm^2). The disk was contained in a low dead-volume (0.4 cm^3) infrared cell which has an optical path length of 2.4 mm (49). The cell temperature was measured by a chromel alumel thermocouple (Omega) and maintained by an electrical resistance heater connected to an Omega series CN-2010 programmable temperature controller. Purified gases were delivered to the infrared cell via Tylan model FC-280 mass flow controllers and analysis of the effluent gas compositions was accomplished with a quadrupole mass spectrometer (EAI model 250B). Infrared spectra were acquired with a Bio-Rad model FTS-15/80 Fourier transform infrared spectrometer using a narrow-band MCT detector. Typically, 64 spectra were collected at a resolution of 4 cm^{-1} to obtain a good signal-to-noise ratio.

RESULTS

Studies of CO and CO_2 Adsorption

The interactions CO and CO_2 with Rh/SiO_2 were investigated at temperatures between 303 and 573 K. Each experiment was initiated by maintaining the reduced catalyst at 548 K for 15 min a 40 cm^3/min flow of He, after which the catalyst was cooled to room temperature in flowing He. The purpose of this pretreatment is to remove adsorbed hydrogen remaining after the reduction of the catalyst (12, 50). The catalyst was then exposed to either flowing CO or CO_2 for 0.5 h and the temperature was increased linearly at 2 K/min. Infrared spectra were collected every 5 min. Spectra were collected, as well, for a 67-mg disk of SiO_2 exposed to CO or CO_2 under conditions identical to those used for the Rh/SiO_2 catalyst. Subtraction of the spectra recorded for SiO_2 from those recorded for Rh/SiO_2 results was performed in the elimination of both the gas-phase spectrum of the adsorbate and the spectrum of the SiO_2 support. Consequently, only the features associated with species adsorbed on the surface of the Rh particles are visible in the spectra presented below.

Figure 1 shows infrared spectra taken as a function of temperature during the exposure of the catalyst to 250 Torr of CO and 510 Torr of He flowing at a total flow rate of

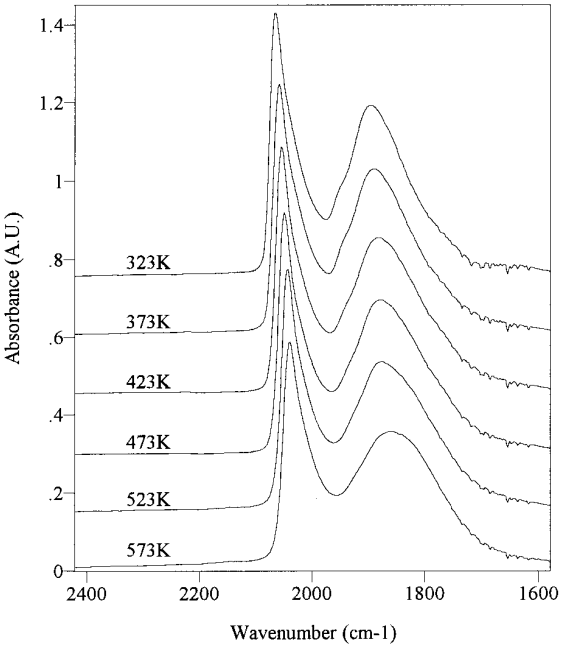

FIG. 1. Infrared spectra for exposure of Rh/SiO_2 to 250 Torr CO and 510 Torr He flowing at a total rate of 35 cm^3/min. Spectra for identical exposure to SiO_2 have been subtracted.

35 cm^3/min. Two principal features are observed at all temperatures. The band centered at 2067–2039 cm^{-1} is assigned to linearly bonded CO on Rh (Rh–CO) and the broad feature centered at 1895–1856 cm^{-1} to bridge-bonded CO on Rh (Rh_2–CO) (15, 24, 29, 31, 51–54). The spectrum recorded at 323 K exhibits a shoulder at 1949 cm^{-1} which becomes less apparent as the temperature is increased. This feature may be assigned to Rh_2–$(CO)_3$ which has the structure shown below (52, 55, 56).

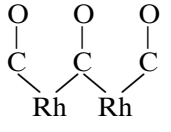

The CO surface coverages of Rh–CO ($\theta_{CO,l}$) and Rh_2–CO ($\theta_{CO,b}$) can be determined by using the integrated Beer–Lambert relation in the form.

$$\theta_{CO,i} = \frac{n_i}{n_{Rh}} = \frac{A_i A_c}{n_{Rh} \varepsilon_i m}, \qquad [1]$$

where

n_i surface concentration of species i [$= \mu$mol/g]
n_{Rh} surface concentration of Rh [$= \mu$mol/g]
A_i integrated absorption intensity for species i [$=$ cm^{-1}]
A_c cross sectional area of catalyst wafer [$=$ cm^2]
ε_i integrated adsorption coefficient [$=$ cm/μmol]
m mass of the catalyst wafer [$=$ g].

The integrated absorption coefficients for linear and bridge bonded CO on Rh used were 13 cm/μmol and 42 cm/μmol,

respectively (52). These values have been shown to be virtually independent of Rh particle size and temperature in the range of 13–58 Å and 323–473 K, respectively. The integrated absorption intensity for Rh_2–$(CO)_3$ was added to that of the bridge bonded species in quantifying $\theta_{CO,b}$ [52].

Figure 2 shows the variation of $\theta_{CO,l}$, $\theta_{CO,b}$, and $\theta_{CO,tot}$ ($\theta_{CO,tot} = \theta_{CO,l} + \theta_{CO,b}$) as a function of temperature. $\theta_{CO,b}$ remains essentially constant while $\theta_{CO,l}$ decreases linearly from 0.82 to 0.71 as the temperature is increased. The small change in $\theta_{CO,tot}$ from 1.19 to 1.08 observed is primarily due to the decrease in $\theta_{CO,l}$ between 303 and 573 K.

Figure 3 shows infrared spectra taken at several different temperatures during the exposure of the catalyst to 250 Torr of CO_2 and 510 Torr of He flowing at a total flow rate of 35 cm^3/min. The band at 2349 cm^{-1} corresponds to weakly adsorbed CO_2 on Rh and is present only in the spectra recorded at temperatures below 523 K. The position of this feature does not vary with temperature. The band appears primarily as a doublet, indicating that the weakly adsorbed CO_2 retains rotational freedom. A similar band at 2350 cm^{-1} has been reported previously for weakly adsorbed CO_2 on Ag/SiO_2 (57), at 2340–2344 cm^{-1} for Cu/SiO_2 (58), and at 2340 cm^{-1} for Rh/SiO_2 (44). The remaining bands are similar to those seen for adsorbed CO and are assumed to arise from the dissociative adsorption of CO_2. The band at 2033–2025 cm^{-1} is assigned to Rh–CO and the broad band at 1822–1800 cm^{-1} to Rh_2–CO. The band at 1901 cm^{-1} is evident at all temperatures and its position is invariant with temperature. This feature is again assigned to Rh_2–$(CO)_3$.

Figure 4 shows the variation of θ_{CO_2}, $\theta_{CO,l}$, $\theta_{CO,b}$, and $\theta_{CO,tot}$ for CO_2 adsorption as a function of temperature. To determine θ_{CO_2}, an integrated absorption coefficient of 13 cm/μmol reported for CO_2 adsorption on Cu/SiO_2 was used (58), since data for Rh are unavailable. Since the heat of CO_2 adsorption on Cu/SiO_2 (~7 kcal/mol) (58) is

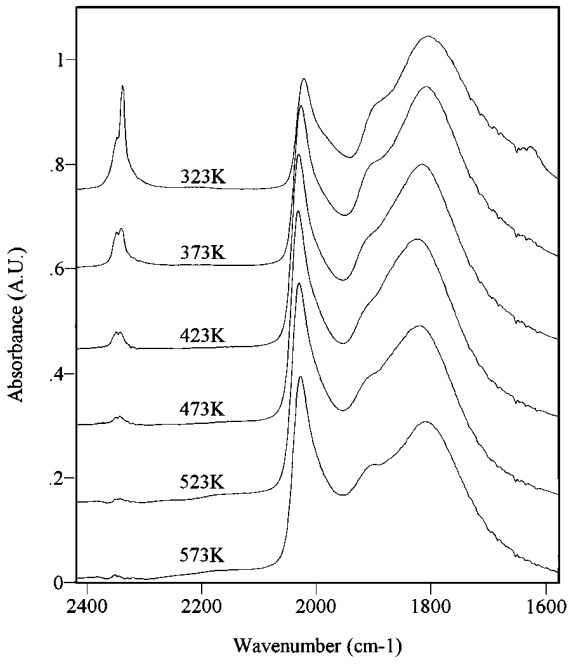

FIG. 3. Infrared spectra for exposure of Rh/SiO_2 to 250 Torr CO_2 and 510 Torr He flowing at a total rate of 35 cm^3/min. Spectra for identical exposure to SiO_2 have been subtracted.

comparable to that determined for Rh/SiO_2 in this study (~6 kcal/mol), the structure of adsorbed CO_2 should be similar, and hence so should the integrated absorption coefficients. θ_{CO_2} decreases monotonically from 0.11 at 314 K to zero at near 500 K. $\theta_{CO,b}$ increases slightly at low temperatures and then remains relatively constant, as in the case of CO adsorption. The magnitude of $\theta_{CO,b}$ is very similar for both CO and CO_2 adsorption. The value of $\theta_{CO,l}$ increases from 0.22 at 303 K to a maximum of 0.58 at 500 K and then decreases at higher temperatures to 0.51. As was the case

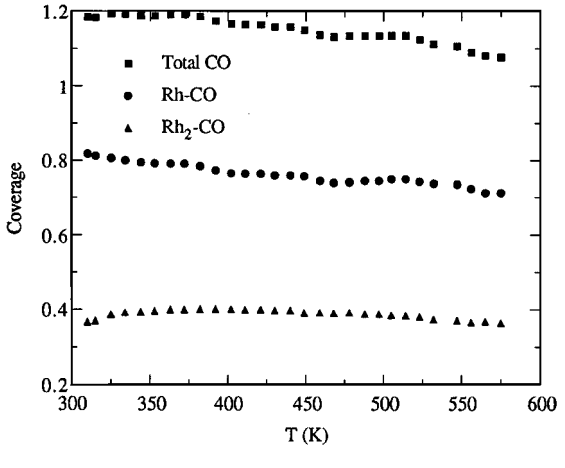

FIG. 2. Temperature dependence of Rh–CO, Rh_2–CO, and total CO surface coverages. Conditions are as in Fig. 1.

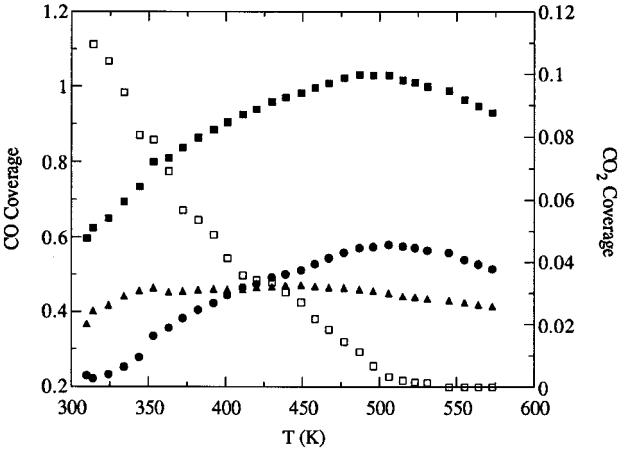

FIG. 4. Temperature dependence of (●) Rh–CO, (▲) Rh_2–CO, (■) total CO, and (□) physisorbed CO_2 surface coverages. Conditions are as in Fig. 3.

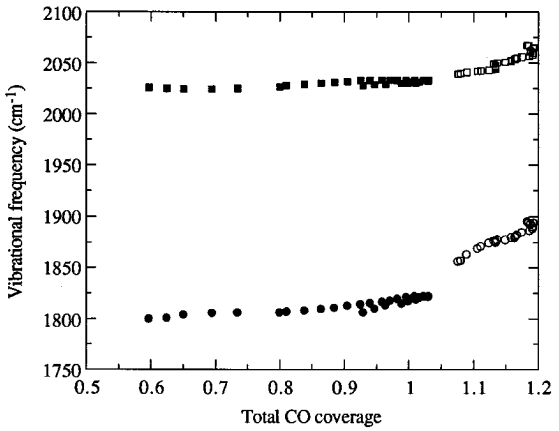

FIG. 5. Coverage dependence of Rh–CO (□, ■) and Rh_2–CO (○, ●) band peak vibrational frequencies resulting from CO (conditions as in Fig. 1) and CO_2 (conditions as in Fig. 3) exposures respectively.

for CO adsorption, the changes in $\theta_{CO,tot}$ with temperature are primarily due to changes in $\theta_{CO,l}$ with temperature.

Figure 5 shows that the vibrational frequencies for both linearly and bridge-bonded CO increase with increasing CO coverage independent of whether the adsorbed CO is derived from the adsorption of CO_2 or CO. The observed change in vibrational frequency with coverage is larger in magnitude for the bridge-bonded species than for the linear species. At low $\theta_{CO,tot}$, $\nu_{CO,l}$ and $\nu_{CO,b}$ are relatively constant, whereas at higher $\theta_{CO,tot}$ both $\nu_{CO,l}$ and $\nu_{CO,b}$ increase significantly. The upscale shift in the vibrational frequency of adsorbed CO with increasing CO coverage is attributable to increased CO dipole–dipole coupling (59), as well as the relative decrease (per CO molecule) in *d*-electron donation from Rh to the π^* antibonding orbital of CO (60). As the total CO surface coverages vary from 0.6 to 1.2, the corresponding frequency shifts are $+42$ cm^{-1} and $+95$ cm^{-1} for the linear and bridge-bonded species, respectively. For CO adsorption on Rh(100), de Jong *et al.* (61) have reported frequency shifts of $+74$ cm^{-1} and $+50$ cm^{-1} for linear and bridge-bonded species, respectively, when increasing the CO coverage from near zero to saturation. They also observed nonlinear frequency shifts with increasing coverages, particularly for the bridged species. On Rh/SiO_2 a frequency shift for linear carbonyls from low to high coverage of $+55$–60 cm^{-1} has been observed for CO adsorption (54).

Reaction Studies

The kinetics of methane formation were investigated in the infrared cell, so that observations of the surface concentrations of adsorbed species could be made concurrently with measurements of the reaction rate. For the range of conditions investigated, the conversion of CO_z never exceeded 2.6%, so that the cell could be considered to be a well-stirred differential reactor. Internal and external heat and mass transfer effects on the overall rate of methane formation were determined to be negligible under the reaction conditions investigated (62).

Figure 6 shows that for fixed partial pressures of H_2 and CO_z the rate of methane formation from CO or CO_2, expressed as a turnover frequency (TOF), obeys an Arrhenius relation. The TOF for methane formation is consistently higher of CO_2 than CO hydrogenation at all temperatures investigated. The apparent activation energies determined from Fig. 6 are 23.3 kcal/mol for CO hydrogenation and 16.6 kcal/mol for CO_2 hydrogenation.

To determine the apparent reaction orders for H_2 and CO_z, experiments were performed at 548 K and 1 atm total pressure with varying partial pressures of H_2 and CO_z. When necessary, helium was used to maintain the total flow rate and total pressure constant. The results of these experiments are shown in Fig. 7. For CO hydrogenation the partial pressure dependences on H_2 and CO are 0.67 and -0.8, respectively, whereas for CO_2 hydrogenation the partial pressure dependences on H_2 and CO_2 are 0.53 and -0.46, respectively.

Figure 8 shows *in situ* infrared spectra taken during the hydrogenation of CO and CO_2 at 473 K and 578 K. Table 1 lists the coverages by different forms of CO, as well as the TOF for methane formation at each temperature. The spectra observed under reaction conditions are qualitatively similar to those recorded when the catalyst is exposed to CO or CO_2 at the same temperature (see Figs. 1 and 3). The only features observed are those for linearly and bridge-bonded CO, in close agreement with what has been reported previously for Rh/SiO_2 (11, 15). As in the case of CO and CO_2 adsorption, the principal difference in the spectra for CO and CO_2 hydrogenation at both temperatures is that $\theta_{CO,tot}$ is larger for CO than for CO_2 hydrogenation. $\theta_{CO,b}$ is again comparable in both reactions and both temperatures, while $\theta_{CO,l}$ is larger for CO than for CO_2 hydrogenation. Table 1 shows that under similar reaction

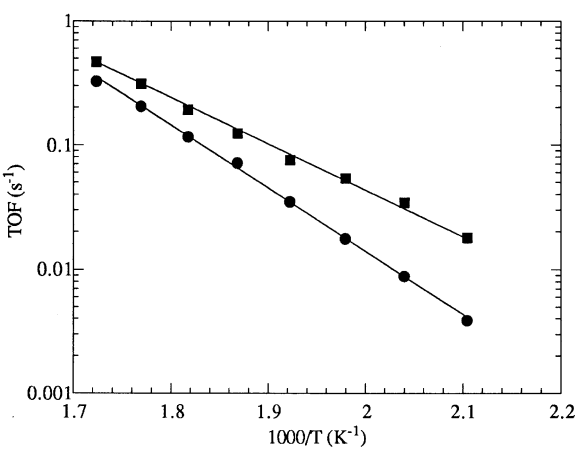

FIG. 6. Arrhenius plots for CO_z hydrogenation. $P_{H_2} = 608$ Torr, $P_{CO_z} = 152$ Torr, and total feed rate = 40 cm^3/min. (■) CO_2, $E_a =$ 16.6 kcal/mol; (●) CO, $E_a = 23.2$ kcal/mol.

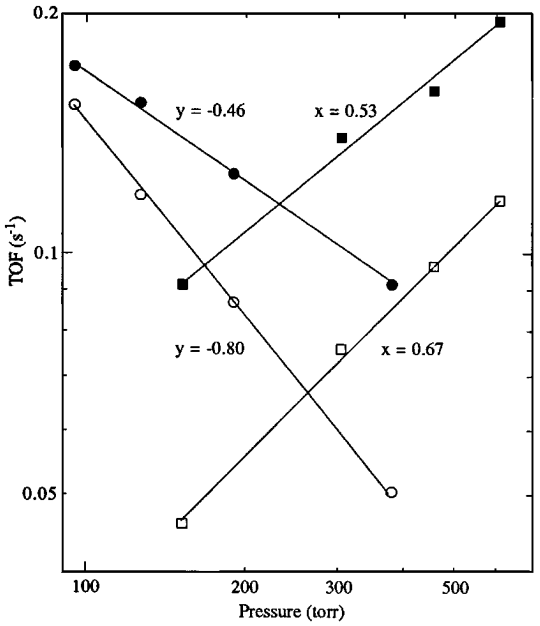

FIG. 7. Reactant partial pressure dependence on the methanation rate for CO_z hydrogenation at 548 K, a total pressure of 760 Torr, and a total feed rate of 40 cm^3/min. $x = H_2$ partial pressure dependence and $y = CO_z$ partial pressure dependence. $P_{H_2} = 380$ Torr, (●) P_{CO_2}, (○) P_{CO}; $P_{CO_z} = 152$ Torr, (■) P_{H_2} $(z = 2)$, (□) P_{H_2} $(z = 1)$.

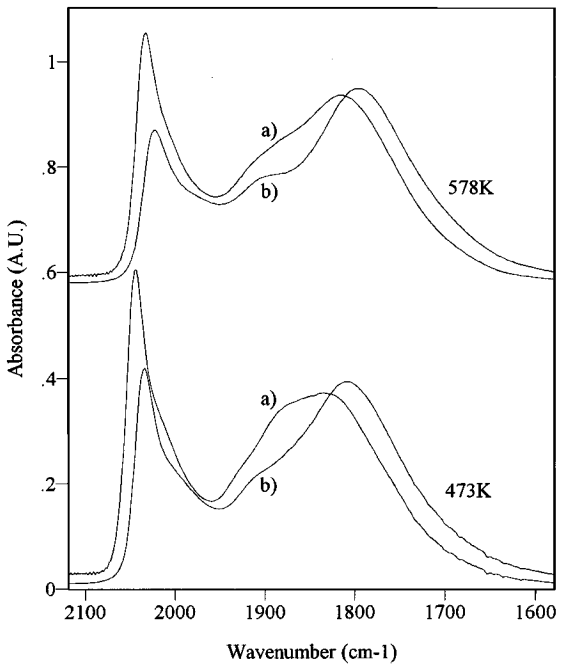

FIG. 8. Infrared spectra taken during CO_z hydrogenation at 473 and 578 K: (a) CO and (b) CO_2. Conditions are as in Fig. 6.

conditions, the rate of CO_2 hydrogenation is higher than the rate of CO hydrogenation, whereas the values of $\theta_{CO,tot}$ exhibit the opposite relationship.

In situ infrared spectra for CO and CO_2 hydrogenation at 548 K and varying reactant partial pressures are shown in Figs. 9 and 10, respectively. Variation of the reactant partial pressures in this range has little effect on the concentrations or vibrational frequencies of the linearly and bridge bonded Rh carbonyls. A slight increase in the CO coverages are observed when the CO_z partial pressure is increased, but increasing the hydrogen partial pressure has no effect on the observed spectra.

Infrared spectra taken under reaction conditions are qualitatively similar to those observed during exposure of the catalyst to CO or CO_2 alone. Quantitative differences are shown in Table 2, which gives a comparison of the spectral features for CO_z hydrogenation and CO_z adsorption at 548 K. Table 2 again shows that at the same feed conditions, $\theta_{CO,tot}$ is higher for CO hydrogenation than for CO_2 hydrogenation, and the resulting methane formation rate is lower for CO than CO_2 hydrogenation. The higher $\theta_{CO,tot}$ is primarily due to the higher $\theta_{CO,l}$ in the case of CO hydrogenation. Table 2 shows that the presence of H_2 decreases $\theta_{CO,l}$ while $\theta_{CO,b}$ increases for both CO and CO_2 hydrogenation as compared to CO and CO_2 adsorption. Although the comparison is made at different CO_z partial pressures, it has been shown that the concentration of adsorbed CO is essentially independent of the CO_z partial pressure (see Figs. 9 and 10). There is a slight increase in $\theta_{CO,tot}$ for both CO and CO_2 in the presence of hydrogen. Table 2 also shows that the positions of all bands are shifted to lower vibrational frequencies during CO_z hydrogenation as compared to CO_z adsorption, even though $\theta_{CO,tot}$ is higher for CO_z hydrogenation than for CO_z adsorption. This trend can be ascribed to electron donation from surface hydrogen, which increases the electron donation from Rh to the π^* antibonding orbital of CO and thereby decreases the C–O bond vibrational frequency (42). The presence of surface hydrogen may also disrupt dipole–dipole coupling of surface CO. The low-frequency shift observed in the presence of hydrogen has been observed previously and has been attributed to the formation of Rh carbonyl hydrides (38, 40–44, 63).

The range of $\theta_{CO,tot}$ accessible to steady-state reaction experiments is limited, since $\theta_{CO,tot}$ is essentially the same for

TABLE 1

Comparison of the Observed Spectral Features and Methane Formation Rates for CO_z Hydrogenation at 473 and 578 K[a]

T (K)	Reactant	$\theta_{CO,tot}$	$\theta_{CO,l}$	$\theta_{CO,b}$	$\nu_{CO,l}$ (cm^{-1})	$\nu_{CO,b}$ (cm^{-1})	TOF (s^{-1})
473	CO $(z = 1)$	1.17	0.70	0.47	2045	1834	0.0039
473	CO_2 $(z = 2)$	1.03	0.54	0.49	2035	1809	0.018
578	CO $(z = 1)$	1.04	0.59	0.45	2035	1817	0.32
578	CO_2 $(z = 2)$	0.89	0.42	0.47	2024	1797	0.47

[a] $P_{H_2} = 608$ Torr, $P_{CO_z} = 152$ Torr, $P_{total} = 760$ Torr, total feed rate = 40 cm^3/min.

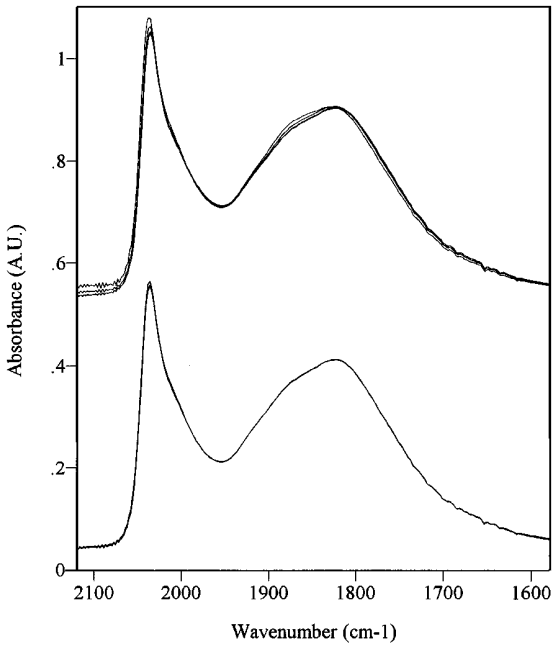

FIG. 9. Infrared spectra taken during CO hydrogenation. Conditions are as in Fig. 7. Top 4 spectra, $P_{H_2} = 380$ Torr and $P_{CO} = 95$, 127, 190, and 380 Torr. Bottom 4 spectra, $P_{CO} = 152$ Torr and $P_{H_2} = 152$, 304, 456, and 608 Torr.

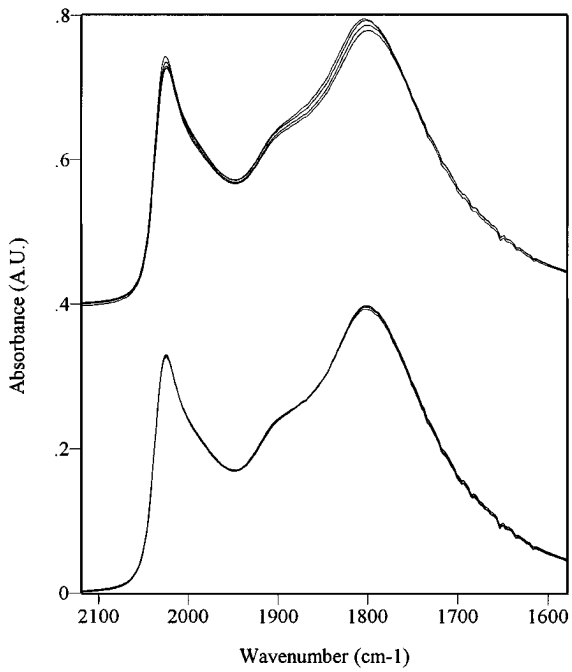

FIG. 10. Infrared spectra taken during CO_2 hydrogenation. Conditions are as in Fig. 7. Top 4 spectra, $P_{H_2} = 380$ Torr and $P_{CO_2} = 95$, 127, 190, and 380 Torr. Bottom 4 spectra, $P_{CO_2} = 152$ Torr and $P_{H_2} = 152$, 304, 456, and 608 Torr.

the range of CO_z partial pressures investigated in this study. To determine how $\theta_{CO,tot}$ affects the rates of CO and CO_2 hydrogenation, transient experiments were performed in which the entire range of CO surface concentrations could be accessed. These experiments were initiated by exposing the reduced catalyst to 1 atm of CO_z flowing at 40 cm^3/min. The infrared spectrum of the surface was monitored until no further increase in CO surface concentration was observed. The feed was then switched to 1 atm hydrogen flowing at 40 cm^3/min and the infrared spectra were collected at 1.5 min intervals while the composition of the reactor effluent was determined every 6 s. The reactor temperature was maintained constant at 548 K throughout the experiment.

The resulting infrared spectra for CO hydrogenation are shown in Fig. 11, and those for CO_2 hydrogenation are shown in Fig. 12. Zero time in both figures corresponds to the moment when the flow was switched from CO_z to hydrogen. Figures 13 and 14 show the variations in $\theta_{CO,l}$, $\theta_{CO,b}$, and $\theta_{CO,tot}$, and the TOF for methane formation as functions of time for CO and CO_2 hydrogenation respectively. For both CO and CO_2, the TOF for methane rises slowly, then accelerates just before reaching a maximum, after which it decreases monotonically. While the maximum TOF, 1.6 s^{-1}, is the same for both CO and CO_2 methanation, the time to reach the maximum is significantly shorter and the initial TOF is 50% higher when CO_2 rather than CO is the reactant. The transients in CO coverage also show differences for the two experiments. For CO hydrogenation $\theta_{CO,b}$ remains nearly constant during the first 13 min of the experiment, whereas $\theta_{CO,l}$ decreases slowly. At 13 min into the transient, the values of $\theta_{CO,l}$ and $\theta_{CO,b}$ become comparable and then decline at the same rate as the experiment progresses further. In the case of CO_2 methanation, the values of $\theta_{CO,l}$ and $\theta_{CO,b}$ are identical at the start of the experiment and decrease at nearly comparable rates as the experiment proceeds, the rate of decrease in $\theta_{CO,b}$ being somewhat slower than that in $\theta_{CO,l}$.

The relationship between the TOF for methane formation and $\theta_{CO,tot}$ for both reaction systems is brought out very clearly in Fig. 15 which shows a plot of TOF versus $\theta_{CO,tot}$. It is evident that over the whole range of CO coverages, the TOFs, for methane formation from CO and CO_2 are very similar at a given CO coverage. This point is further illustrated in Fig. 16 which shows that the spectra for adsorbed CO and the TOF for methane formation are virtually identi-

TABLE 2

Comparison of the Observed Spectral Features for CO_z Hydrogenation and CO_z Adsorption at 548 K

P_{H_2} (Torr)	P_{CO_z} (Torr)	$\theta_{CO,tot}$	$\theta_{CO,l}$	$\theta_{CO,b}$	$\nu_{CO,l}$ (cm^{-1})	$\nu_{CO,b}$ (cm^{-1})	TOF (s^{-1})
608	152 ($z = 1$)	1.13	0.67	0.46	2037	1823	0.12
608	152 ($z = 2$)	1.00	0.49	0.51	2025	1803	0.20
—	250 ($z = 1$)	1.08	0.71	0.37	2042	1869	—
—	250 ($z = 2$)	0.99	0.56	0.43	2030	1815	—

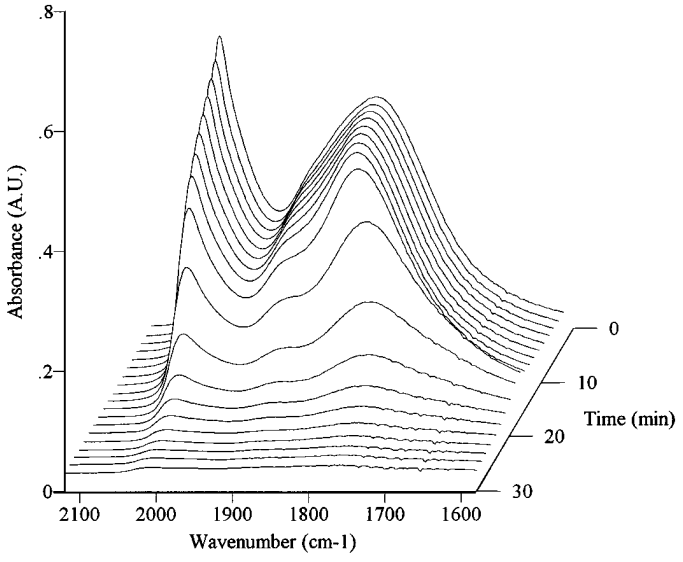

FIG. 11. Infrared spectra taken during the hydrogenation of CO surface species. Catalyst exposed to 760 Torr CO. Feed then switched to 760 Torr H_2. Time = 0 is the time of the feed switch from CO to H_2.

cal when observed at an identical value of $\theta_{CO,tot}$. Figure 15 demonstrates, as well, that the TOF for methane formation passes through a maximum at a total CO coverage of about 0.7.

DISCUSSION

Studies of CO and CO_2 Adsorption

Under the conditions used in this study, CO adsorption on Rh produces linearly and bridge-bonded carbonyls. The

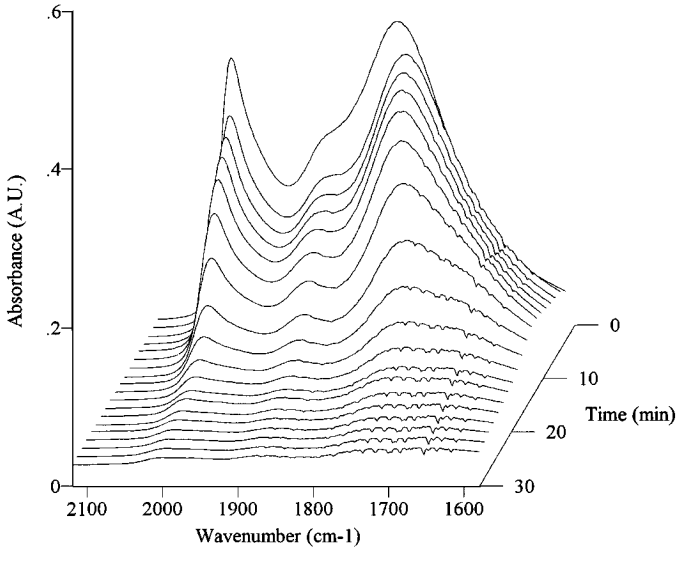

FIG. 12. Infrared spectra taken during the hydrogenation of CO surface species. Catalyst exposed to 760 Torr CO_2. Feed was then switched to 760 Torr H_2. Time = 0 is the time of the feed switch from CO_2 to H_2.

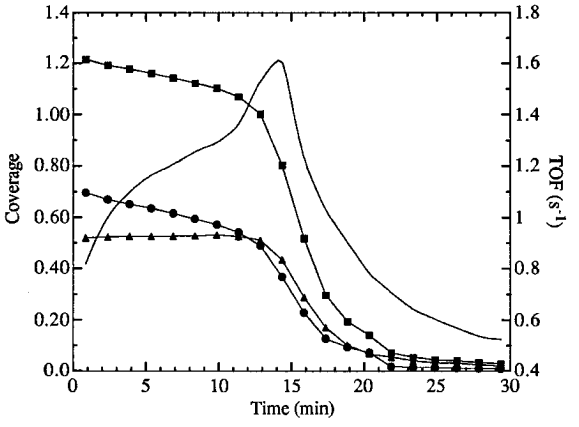

FIG. 13. Transient response of CO species coverage and the methane formation rate for the hydrogenation of adsorbed CO resulting from CO exposure. Conditions are as in Fig. 11. (■) Total CO, (●) Rh–CO, (▲) Rh_2–CO, (—) TOF.

results presented in Fig. 2 indicate that Rh–CO is more weakly bound than the bridge-bonded species, since with increasing temperature the surface coverage of Rh–CO decreases while that of the bridge-bonded species remains essentially constant. This observation is in agreement with studies of CO adsorption on Rh/Al_2O_3, which have also shown Rh–CO to be less stable than Rh_2–CO (55, 64). We observe a maximum total CO coverage of 1.2 (Fig. 2). The corresponding observed maximum coverage of linear carbonyls is 0.8 and that of the bridge-bonded species is 0.4. A total CO coverage greater than unity results from the contribution of Rh_2–$(CO)_3$ to the overall stoichiometry. CO coverages in excess of unity are well know and have been reported to be as high as 2 for highly dispersed Rh catalysts where Rh dicarbonyl (Rh–$(CO)_2$) formation dominates (39, 65, 66).

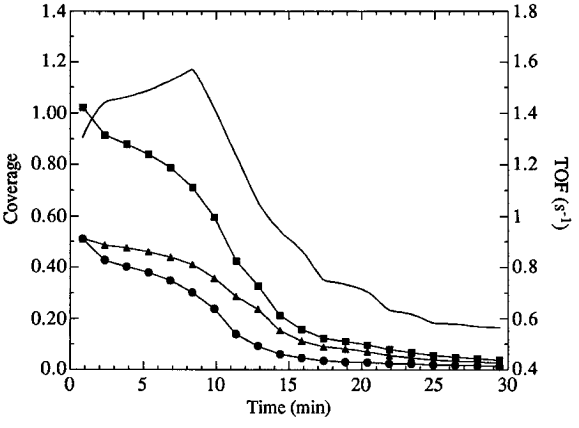

FIG. 14. Transient response of CO species coverage and the methane formation rate for the hydrogenation of adsorbed CO resulting from CO_2 exposure. Conditions are as in Fig. 12. (■) Total CO, (●) Rh–CO, (▲) Rh_2–CO, (—) TOF.

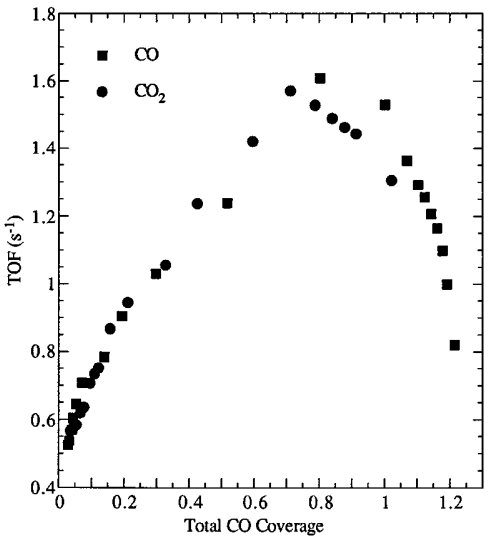

FIG. 15. Dependence of the methane formation rate on CO surface coverage for CO_z hydrogenation. Conditions are as in Fig. 11 for (■) CO hydrogenation and Fig. 12 for (●) CO_2 hydrogenation.

When Rh/SiO_2 is exposed to CO_2, linearly and bridge-bonded CO are observed together with weakly adsorbed CO_2. Figure 4 shows that with increasing temperature the coverage of CO_2 decreases monotonically. If it is assumed that CO_2 adsorption is at equilibrium, the apparent heat of adsorption can be estimated from a plot of $\ln \theta_{CO2}$ vs $1/T$. The heat of CO_2 adsorption determined by this means is 6 kcal/mol. This result is in good agreement with an activation energy of 6.5 kcal/mol for the desorption of physically adsorbed CO_2 from a Rh tip (67). Figure 4 also shows that the coverage of bridge-bonded CO remains nearly independent of temperature at a value of about 0.4, while the coverage by linearly adsorbed CO increases and passes through a maximum. This indicates that, as in CO adsorption, the bridge-bonded species are thermally more stable than linear species. The trends observed in Fig. 4 suggest that adsorbed CO_2 dissociates to produce adsorbed CO. Since bridge-bonded CO is more strongly bound than linearly adsorbed CO, the sites for bridge-bounded CO are saturated. With increasing temperature the total amount of adsorbed CO increases initially due to the more rapid rate of CO_2 dissociation. The decrease in CO coverage above 500 K is attributed to the reduced rate of CO_2 dissociation associated with the drop in the CO_2 coverage to nearly zero, as well as more rapid CO desorption. The overall chemistry of CO_2 interacting with the surface of Rh between 303 K and 573 K can then be summarized as follows:

$$CO_{2,g} \rightleftharpoons CO_{2,s} \rightleftharpoons \begin{matrix} CO_g \\ \Downarrow \\ CO_s \end{matrix} + O_s$$

While the data presented here clearly indicate evidence for CO_2 dissociation on Rh/SiO_2, the question of whether or not CO_2 dissociates on Rh is still a subject of discussion in the literature. CO_2 dissociation on Rh foils and on Rh single crystals has been reported by a number of investigators (1, 67–73). In a study of the effect of surface structure, Hendrickx *et al.* (67, 71) noted that CO_2 adsorption occurs more readily on open crystal planes such as (210), (320), and (531), and that the most active sites for CO_2 dissociation are located along the steps between (111) or (100) surfaces. By contrast, Solymosi and co-workers have reported that CO_2 dissociation does not occur on Rh foils and single crystals (74–77) or on Rh supported on Al_2O_3 or SiO_2 (41, 44) and have suggested that the observation of CO_2 dissociation may be facilitated by adsorbed hydrogen (41) and impurities such as boron (78). A low probability of CO_2 dissociation on close-packed surfaces is also suggested by theoretical calculations performed by Weinberg (79). The presence of adsorbed hydrogen is not likely to be important in the work presented here, since a conscious effort was made to remove any adsorbed hydrogen remaining on the catalyst surface after reduction.

In the scheme shown above, no provision is made for the dissociation of adsorbed CO. This step can be excluded based on the published literature. Thermal dissociation of CO has been found to negligible on Rh(111) at temperatures as high as 870 K (80), nor could dissociation be observed on a Rh field emission tip in CO pressures up to 10^{-1} Torr and temperatures up to 1000 K (81). Similarly, no

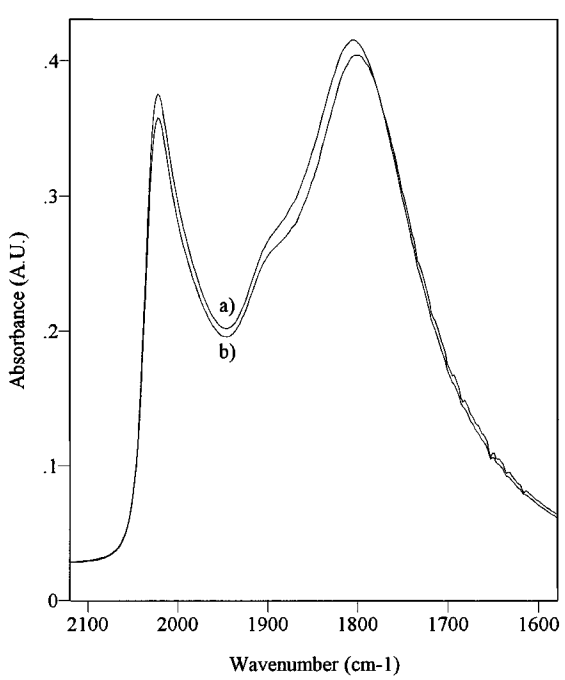

FIG. 16. Comparison of IR spectra at similar CO surface coverages taken during (a) CO hydrogenation and (b) CO_2 hydrogenation. (a) $\theta_{CO} = 1.07$, TOF = 1.36 s^{-1} and (b) $\theta_{CO} = 1.02$, TOF = 1.30 s^{-1}. Conditions are as in Fig. 11 for CO hydrogenation and Fig. 12 for CO_2 hydrogenation.

TABLE 3

Comparison of the Power Law[a] Rate Parameters for CO_z Hydrogenation on Rh Catalysts

Catalyst	E_a (kcal/mol)	x	y	Reference
	$H_2 + CO$ reaction			
3.4 wt% Rh/SiO_2	23.2	0.67	−0.80	This work
1 wt% Rh/SiO_2	22.6	0.57	−0.20	18
4.6 wt% Rh/SiO_2	23	0.6	0.1	88
2.3 wt% Rh/SiO_2	28.5	—	0	27
1 wt% Rh/Al_2O_3	24.0	0.90	−0.42	18
1 wt% Rh/Al_2O_3	24.0	1.04	−0.20	7
Rh foil	24	1	−1	6
Rh foil	24	—	—	1
	$H_2 + CO_2$ reaction			
3.4 wt% Rh/SiO_2	16.6	0.53	−0.46	This work
5 wt% Rh/SiO_2	17.3	0.64	0.27	42
2.3 wt% Rh/SiO_2	15.9	—	0.4	27
1.047 wt% Rh/SiO_2	23.7	—	—	39
5 wt% Rh/Al_2O_3	16.2	0.61	0.26	42
5 wt% Rh/Al_2O_3	16.2	—	—	40
Rh foil	17	0.5	0.2	35
Rh foil	16	—	—	1

[a] $TOF_{CH_4} = Ae^{-E_a/RT} P_{H_2}^x P_{CO_z}^y$.

evidence of CO dissociation has been reported for Rh/SiO_2 at temperatures between 300 and 723 K (12). While a small amount of CO_2 formation has been observed at temperatures above 473 K upon exposure of supported Rh catalysts to CO (19), subsequent work (82) suggests that this product arises from the reaction of CO with hydroxyl groups on the support, rather than from CO disproportionation.

Reaction Studies

The power-law rate parameters obtained from the present experiments are summarized in Table 3 and compared with those reported in the literature. The apparent activation energies determined for both reactions are generally in good agreement with other reported values regardless of the nature of the catalyst. Among Rh/SiO_2 catalysts, the hydrogen partial pressure dependences for both reactions are in good agreement, while the CO_z partial pressure dependences are more variable, ranging from −0.80 to 0.1 for CO hydrogenation and from −0.46 to 0.4 for CO_2 hydrogenation. The negative dependences on the partial pressures of CO and CO_2 observed in this study are fully consistent with the *in situ* infrared observations. Figures 9 and 10 show that increasing the CO_z partial pressure from 95 Torr to 380 Torr at a constant hydrogen partial pressure results in only a slight increase in the total CO coverage but a significant decrease in the TOF for methane formation (see Fig. 7). Figure 15 also shows that, at high total CO coverages, an increase in total CO coverage results in a decrease in the TOF for methane formation. From these results it is apparent that at high total CO coverages (>0.7), an increase in CO_z partial pressure results in an increased total CO coverage and a corresponding decrease in the methane formation rate, and hence the negative dependence on CO_z partial pressure is observed. It should be noted that at lower total CO coverages (<0.7), Fig. 15 shows that an increase in CO_z partial pressure resulting in an increased total CO coverage would correspond to an increase in the methane formation rate, and a positive dependence on CO_z partial pressure should be observed. Moreover, near the maximum in Fig. 15 a zero-order dependance on CO_z partial pressure is expected. This may explain the spread in CO_z partial pressure dependances for CO and CO_2 hydrogenation reported in the literature (see Table 3). The more negative partial pressure dependance on CO as compared to CO_2 observed in the present study is also consistent with the results in Fig. 15. When CO is hydrogenated at steady-state the total CO coverage is higher ($\theta_{CO,tot} \sim 1.13$) than when CO_2 is hydrogenated at equivalent conditions ($\theta_{CO,tot} \sim 1$; see Table 2). Figure 15 shows that increases in CO coverage around $\theta_{CO,tot} = 1.13$ cause a more significant decrease in the TOF for methane formation than similar changes in CO coverage at $\theta_{CO,tot} = 1$, and hence a more negative partial pressure dependance is observed for CO than CO_2.

We have observed that, under equivalent reaction conditions, the TOF for methane formation is higher for CO_2 hydrogenation than for CO hydrogenation (see Tables 1 and 2, Figs. 6 and 7), in agreement with previous comparative investigations involving Rh catalysts (1, 4, 26, 27, 35, 38, 40, 42). Several authors have suggested that this activity difference is related to the higher CO surface coverage during CO hydrogenation as compared to CO_2 hydrogenation (26, 27, 35, 38, 42). We have provided quantitative evidence which supports this view. Tables 1 and 2 show that under equivalent reaction conditions the higher surface coverage of CO observed during CO hydrogenation correlates with a lower TOF for methane formation as compared to CO_2 hydrogenation. We have also shown that when the CO surface coverage is equivalent, rather than at the gas phase partial pressures, the TOF for methane formation is equivalent for both CO and CO_2 hydrogenation (see Figs. 15 and 16). This evidence strongly suggests that the observed activity differences for CO and CO_2 hydrogenation are due to differences in the CO surface coverage.

Mechanism for CO and CO_2 Hydrogenation to Methane

It is generally agreed that for Rh the dissociation of the C–O bond is the rate-limiting step for CO hydrogenation, and that the mechanism for CO_2 hydrogenation is similar to that for CO hydrogenation. Less generally agreed upon is whether C–O bond cleavage occurs via the direct dissociation of adsorbed CO or via a hydrogen-assisted process. Several authors provide evidence supporting hydrogen assisted C–O bond dissociation and these investigations are briefly summarized below.

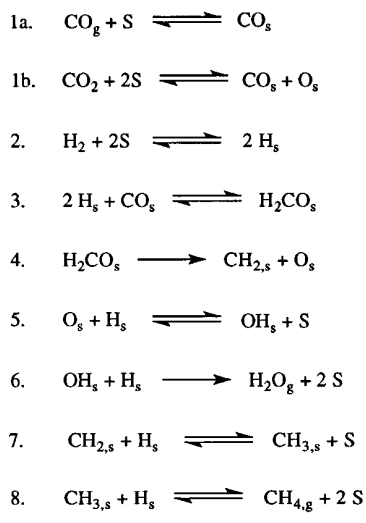

FIG. 17. Proposed mechanism for CO and CO_2 hydrogenation (35, 85).

Vannice (7) has proposed that the dissociation of adsorbed enol species, CHOH, is the rate-limiting step in CO hydrogenation on various group VIII metals. This species was assumed to be formed from the reaction of adsorbed CO and adsorbed hydrogen. Rate expressions derived from this rate limiting step were shown to be consistent with those observed experimentally. More recently, Mori *et al.* (20, 21, 83) have suggested that the rate limiting step for CO hydrogenation is the dissociation of H_nCO, where $n = 1$, 2, or 3. This proposal was made based on the observation of an inverse isotope effect during the reaction of CO with hydrogen as compared to deuterium. Further support for the hydrogen-assisted dissociation of CO comes from the observations of methane formation at temperatures lower than those required for CO dissociation in the absence of hydrogen (24). Also, several works have suggested that CO dissociation is assisted by hydrogen through the formation of a carbonyl hydride which weakens the C–O bond relative to the carbonyl (18, 38, 42). BOC–MP calculations have also shown that the dissociation of H_nCO, where $n = 1$, 2, or 3, is energetically more favorable than the direct dissociation of CO on Pd and Pt (84). Although there is significant evidence to support the idea that C–O bond cleavage is hydrogen assisted, no direct evidence for the existence of H_nCO surface species during the hydrogenation of CO or CO_2 has been reported.

Williams *et al.* (35, 85) have proposed a mechanism for CO and CO_2 hydrogenation to methane over Rh based on the observations reported above. As shown in Fig. 17, the sequence begins with the adsorption of CO in the case of CO hydrogenation, of the dissociative adsorption of CO_2 in the case of CO_2 hydrogenation. Adsorbed CO is then hydrogenated to produce surface formaldehyde, which subsequently dissociates to form $CH_{2,s}$ and O_s. The dissociation of adsorbed formaldehyde is assumed to be the rate-determining step. $CH_{2,s}$ species produced in step 4 undergo hydrogenation to form methane, whereas O_s undergoes hydrogenation to form water. Although adsorbed formaldehyde has not been observed under reaction conditions, the reverse of reaction 3 has been observed at 295 K upon exposure of Rh/Al_2O_3 to H_2CO (86).

An expression for the rate of methane formation from either CO or CO_2 can be determined from the mechanism in Fig. 17. In so doing, it is assumed that adsorbed hydrogen and CO are the most abundant surface species, and that the steps prior to the rate-determining step are equilibrated. The resulting rate expression is given by

$$\mathrm{TOF}_{CH_4} = \frac{k_4 K_2 K_3}{1 + K_2^{1/2} P_{H_2}^{1/2}} P_{H_2} [\theta_{CO,tot}(\theta_{max} - \theta_{CO,tot})], \quad [2]$$

where θ_{max} is the maximum surface occupancy by all adsorbed species. In deriving Eq. [2], it is assumed that H_2 and CO compete for adsorption sites, but no distinction is made between different forms of adsorbed CO. This is clearly a simplification, since the transient response data presented in Figs. 13 and 14 suggest that linearly adsorbed CO reacts preferentially to bridge-bonded CO.

Equation [2] suggests that the partial pressure dependence on H_2 should lie between 1 and 1/2, if it is assumed that $\theta_{CO,tot}$ is independent of H_2 partial pressure, an assumption that is well supported by the infrared results presented in Figs. 9 and 10. Experiments conducted with unsupported Rh black (87) have shown that during CO hydrogenation under conditions similar to those used in the present study, a large fraction of the sites available for H_2 chemisorption are occupied. This would suggest that $(K_2 P_{H_2})^{1/2} > 1$ and, hence, that the apparent order in H_2 should be closer to 0.5 than 1, consistent with what is found experimentally (see Table 3).

At constant hydrogen partial pressure and temperature, Eq. [2] predicts that a maximum in the methane formation rate should be observed at intermediate CO coverages and that the rate should fall to zero as the CO surface concentration approaches either 0 or θ_{max}. Moreover, the rate expression predicts that at the same hydrogen partial pressure, temperature, and CO surface concentration, the methane formation rate should be the same for both CO and CO_2 hydrogenation. The results shown in Figs. 15 and 16 closely agree with these predictions. The asymmetry in the plot of TOF versus $\theta_{CO,tot}$ seen in Fig. 15 may be attributable to the coverage dependance of the rate constant and equilibrium constants in Eq. [2].

Equation [2] also helps to explain the dependence of the steady-state rates of methane formation on the partial pressures of CO and CO_2, as well as the differences in apparent activation energies for CO and CO_2 hydrogenation. For CO or CO_2 partial pressures between 95 and 380 Torr Figs. 9 and 10 show that the CO coverage is near the maximum and increases only slightly as the partial pressure of either CO or CO_2 is increased. Equation [2] shows that under these

circumstances, the rate of methane formation will decrease with increasing CO_z partial pressure due to the behavior of the factor in brackets, consistent with the negative partial dependances observed for both CO and CO_2 hydrogenation (see Table 3). The data in Fig. 6 indicate that the apparent activation energy is 6.6 kcal/mol larger for CO than for CO_2 methanation. Inspection of Eq. [2] indicates that this difference must arise from the temperature dependence of the factor $\theta_{CO,tot}(\theta_{max}-\theta_{CO,tot})$, since the remaining factors are the same for CO and CO_2 hydrogenation. If θ_{max} is taken to be 1.4, the difference in the apparent activation energies determined by plotting $\ln[\theta_{CO,tot}(\theta_{max}-\theta_{CO,tot})]$ versus 1/T is 6.5 kcal/mol. A value of 1.4 for θ_{max} is reasonably obtained upon extrapolation of the data in Fig. 15 to zero TOF. Thus, Eq. [2] provides a satisfactory basis for describing the rates of methane formation from CO and CO_2 under both steady-state and transient-response conditions.

CONCLUSIONS

For equivalent reactant partial pressures and reaction temperature, the rate of methane formation over Rh/SiO_2 is higher for CO_2 than for CO hydrogenation. The activation energy for CO_2 hydrogenation is smaller than that for CO hydrogenation by 6.6 kcal/mol. Both reactions exhibit a roughly half-order dependence on H_2 partial pressure and an inverse order dependence on the partial pressure of CO_z ($z = 1, 2$). *In situ* infrared spectroscopy reveals that the surface is covered practically to saturation by a combination of linearly and bridge-bonded CO. The total CO coverage is higher during CO hydrogenation than CO_2 hydrogenation. Over the range of conditions examined, the CO coverage during reaction is independent of the H_2 partial pressure and increases only slightly with increasing CO_z partial pressure.

Transient-response experiments combined with *in situ* infrared spectroscopy demonstrate that adsorbed CO, derived from the adsorption of CO or the dissociative adsorption of CO_2, reacts with hydrogen to form methane and that the rate of methane formation passes through a maximum as the CO coverage decreases from saturation to zero. The mechanisms by which CO and CO_2 undergo hydrogenation are envisioned to be very similar. In both cases hydrogenation of adsorbed CO to form H_2CO is followed by the dissociation of this product to release CH_2 species which then undergo further hydrogenation to form methane. The only difference between CO and CO_2 hydrogenation is that in the latter case CO_2 must first dissociate. Confirmation of the dissociative adsorption of CO_2 was obtained from examination of the interactions of CO_2 with Rh. The rate expression derived from the mechanism correctly describes most of the features of the reaction kinetics observed experimentally under both steady-state and transient conditions.

ACKNOWLEDGMENTS

The authors acknowledge Z. Weng-Sieh for obtaining transmission electron micrographs of the catalyst used in this study. This work was supported by the Director, Office of Energy Research, Office of Basic Energy Sciences, Chemical Sciences Division of the U.S. Department of Energy under Contract DE-AC03-76SF00098.

REFERENCES

1. Sexton, B. A., and Somorjai, G. A., *J. Catal.* **46**, 167 (1977).
2. Castner, D. G., Blackadar, R. L., and Somorjai, G. A., *J. Catal.* **66**, 257 (1980).
3. Williams, K. J., Boffa, A. B., Lahtinen, J., Salmeron, M., Bell, A. T., and Somorjai, G. A., *Catal. Lett.* **5**, 385 (1990).
4. Boffa, A. B., Bell, A. T., and Somorjai, G. A., *J. Catal.* **139**, 602 (1993).
5. Boffa, A. B., Lin, C., Bell, A. T., and Somorjai, G. A., *J. Catal.* **149**, 149 (1994).
6. Levin, M. E., Salmeron, M., Bell, A. T., and Somorjai, G. A., *J. Chem. Soc. Faraday Trans. 1* **83**, 2061 (1987).
7. Vannice, M. A., *J. Catal.* **37**, 449 (1975).
8. Siddall, J. H., Miller, M. L., and Delgass, W. N., *Chem. Eng. Comm.* **83**, 261 (1989).
9. McQuire, M. W., and Rochester, C. H., *Ber. Bunsenges. Phys. Chem.* **97**, 298 (1993).
10. Koerts, T., Welters, W. J. J., and van Santen, R. A., *J. Catal.* **134**, 1 (1992).
11. Balakos, M. W., Chuang, S. S. C., and Srinivas, G., *J. Catal.* **140**, 281 (1993).
12. Ioannides, T., and Verykios, X., *J. Catal.* **140**, 353 (1993).
13. Borer, A. L., Brönnimann, C., and Prins, R., *J. Catal.* **145**, 516 (1994).
14. Efstathiou, A. M., Chafik, T., Bianchi, D., and Bennett, C. O., *J. Catal.* **148**, 224 (1994).
15. Lavalley, J. C., Saussey, J., Lamotte, J., Breault, R., Hindermann, J. P., and Kiennemann, A., *J. Phys. Chem.* **94**, 5941 (1990).
16. Demri, D., Hindermann, J. P., and Kiennemann, A., *Catal. Lett.* **23**, 277 (1994).
17. Underwood, R. P., and Bell, A. T., *Appl. Catal.* **21**, 157 (1986).
18. Solymosi, F., Tombácz, I., and Kocsis, M., *J. Catal.* **75**, 78 (1982).
19. Erdöhelyi, A., and Solymosi, F., *J. Catal.* **84**, 446 (1983).
20. Mori, Y., Mori, T., Miyamoto, A., Takahashi, N., Hattori, T., and Murakami, Y., *J. Phys. Chem.* **93**, 2039 (1989).
21. Mori, Y., Mori, T., Hattori, T., and Murakami, Y., *J. Phys. Chem.* **94**, 4575 (1990).
22. Lisitsyn, A. S., Stevenson, S. A., and Knözinger, H., *J. Mol. Catal.* **63**, 201 (1990).
23. Alekseev, O. S., Beutel, T., Paukshtis, E. A., Ryndin, Y. A., Likholobov, V. A., and Knözinger, H., *J. Mol. Catal.* **92**, 217 (1994).
24. Sachtler, W. M. H., and Ichikawa, M., *J. Phys. Chem.* **90**, 4752 (1986).
25. Fujimoto, K., Kameyama, M., and Kunugi, T., *J. Catal.* **61**, 7 (1980).
26. Iizuka, T., Tanaka, Y., and Tanabe, K., *J. Mol. Catal.* **17**, 381 (1982).
27. Iizuka, T., Tanaka, Y., and Tanabe, K., *J. Catal.* **76**, 1 (1982).
28. Inoue, T., Iizuka, T., and Tanabe, K., *Appl. Catal.* **46**, 1 (1989).
29. de Jong, K. P., Glezer, J. H. E., Kuipers, H. P. C. E., Knoester, A., and Emeis, C. A., *J. Catal.* **124**, 520 (1990).
30. Burch, R., and Petch, M. I., *Appl. Catal. A* **88**, 77 (1992).
31. Luo, H., Zhou, H., Lin, L., Liang, D., Li, C., Fu, D., and Xin, Q., *J. Catal.* **145**, 232 (1994).
32. Ioannides, T., Verykios, X. E., Tsapatsis, M., and Economou, C., *J. Catal.* **145**, 491 (1994).
33. van der Lee, G., Schuller, B., Post, H., Favre, T. L. F., and Ponec, V., *J. Catal.* **98**, 522 (1986).
34. Kiennemann, A., Breault, R., Hindermann, J. P., and Laurin, M., *J. Chem. Soc. Faraday Trans. 1* **83**, 2119 (1987).

35. Williams, K. J., Boffa, A. B., Salmeron, M., Bell, A. T., and Somorjai, G. A., *Catal. Lett.* **9**, 415 (1991).
36. Amariglio, A., Lakhdar, M., and Amariglio, H., *J. Catal.* **81**, 247 (1983).
37. Benitez, J. J., Alvero, R., Capitán, M. J., Carrizosa, I., and Odriozola, J. A., *Appl. Catal.* **71**, 219 (1991).
38. Henderson, M. A., and Worley, S. D., *J. Phys. Chem.* **89**, 1417 (1985).
39. Ichikawa, S., *J. Mol. Catal.* **53**, 53 (1989).
40. Solymosi, F., and Erdöhelyi, A., *J. Mol. Catal.* **8**, 471 (1980).
41. Solymosi, F., Erdöhelyi, A., and Kocsis, M., *J. Catal.* **65**, 428 (1980).
42. Solymosi, F., Erdöhelyi, A., and Bánsági, T., *J. Catal.* **68**, 371 (1981).
43. Solymosi, F., and Pásztor, M., *J. Catal.* **104**, 312 (1987).
44. Solymosi, F., and Knözinger, H., *J. Catal.* **122**, 166 (1990).
45. Trovarelli, A., Mustazza, C., and Dolcetti, G., *Appl. Catal.* **65**, 129 (1990).
46. Kai, T., Matsumura, T., and Takahashi, T., *Catal. Lett.* **16**, 129 (1992).
47. Zhang, Z., Kladi, A., and Verykios, X. E., *J. Catal.* **148**, 737 (1994).
48. Nozaki, F., Sodesawa, T., Sahtoh, S., and Kimura, K., *J. Catal.* **104**, 339 (1987).
49. Hicks, R. F., Kellner, C. S., Savatsky, B. J., Hecker, W. C., and Bell, A. T., *J. Catal.* **71**, 216 (1981).
50. Gorodetskii, V. V., Nieuwenhuys, B. E., Sachtler, W. M. H., and Boreskov, G. K., *Surf. Sci.* **108**, 225 (1981).
51. Kraus, L., Zaki, M. I., and Knözinger, H., *J. Mol. Catal.* **55**, 55 (1989).
52. Rasband, P. B., and Hecker, W. C., *J. Catal.* **139**, 551 (1993).
53. Bredikhin, M. N., Lokhov, Y. A., and Kuznetsov, V. L., *Kinetics and Catal.* **28**, 585 (1987).
54. Angevaare, P. A. J. M., Hendrickx, H. A. C. M., and Ponec, V., *J. Catal.* **110**, 18 (1988).
55. Yang, A. C., and Garland, C. W., *J. Phys. Chem.* **61**, 1504 (1957).
56. Rice, C. A., Worley, S. D., Curtis, C. W., Guin, J. A., and Tarrer, A. R., *J. Chem. Phys.* **74**, 6487 (1981).
57. Force, E. L., and Bell, A. T., *J. Catal.* **38**, 440 (1975).
58. Clarke, D. B., Suzuki, I., and Bell, A. T., *J. Catal.* **142**, 27 (1993).
59. Sheppard, N., and Nguyen, T. T., *in* "Advances in Infrared and Raman Spectroscopy," Vol. 5, Chap. 2. Heyden, London/New York, 1975.
60. Blyholder, G., *J. Phys. Chem.* **68**, 2772 (1964).
61. de Jong, A. M., and Niemantsverdriet, J. W., *J. Chem. Phys.* **101**, 10126 (1994).
62. Kapteijn, F., Marin, G. B., and Moulijn, J. A., *in* "Catalysis: An Integrated Approach to Homogeneous, Heterogeneous, and Industrial Catalysis," Studies in Surface Science and Catalysis, Vol. 79, Chap. 7. Elsevier, Amsterdam, 1993.
63. Mckee, M. L., Dai, C. H., and Worley, S. D., *J. Phys. Chem.* **92**, 1056 (1988).
64. Yao, H. C., and Rothschild, W. G., *J. Chem. Phys.* **68**, 4774 (1978).
65. van't Blik, H. F. J., van Zon, J. B. A. D., Huizinga, T., Vis, J. C., Koningsberger, D. C., and Prins, R., *J. Am. Chem. Soc.* **107**, 3139 (1985).
66. Yao, H. C., Japar, S., and Shelef, M., *J. Catal.* **50**, 407 (1977).
67. Hendrickx, H. A. C. M., Jongenelis, A. P. J. M., and Nieuwenhuys, B. E., *Surf. Sci.* **154**, 503 (1985).
68. Castner, D. G., Sexton, B. A., and Somorjai, G. A., *Surf. Sci.* **71**, 519 (1978).
69. Dubois, L. H., and Somorjai, G. A., *Surf. Sci.* **88**, L213 (1979).
70. Dubois, L. H., and Somorjai, G. A., *Surf. Sci.* **91**, 514 (1980).
71. Hendrickx, H. A. C. M., Jongenelis, A. P. J. M., and Nieuwenhuys, B. E., *Surf. Sci.* **162**, 269 (1985).
72. van Tol, M. F. H., Gielbert, A., and Nieuwenhuys, B. E., *Appl. Surf. Sci.* **67**, 166 (1993).
73. van Tol, M. F. H., Gielbert, A., Wolf, R. M., Lie, A. B. K., and Nieuwenhuys, B. E., *Surf. Sci.* **287/288**, 201 (1993).
74. Solymosi, F., and Kilvényi, G., *Surf. Sci.* **315**, 255 (1994).
75. Solymosi, F., and Kiss, J., *Surf. Sci.* **149**, 17 (1985).
76. Solymosi, F., and Bugyi, L., *J. Chem. Soc. Faraday Trans. I* **83**, 2015 (1987).
77. Solymosi, F., and Kilvényi, G., *Catal. Lett.* **22**, 337 (1993).
78. Solymosi, F., *J. Mol. Catal.* **65**, 337 (1991).
79. Weinberg, W. H., *Surf. Sci.* **128**, L224 (1983).
80. Yates, J. T., Williams, E. D., and Weinberg, W. H., *Surf. Sci.* **91**, 562 (1980).
81. Gorodetskii, V. V., and Nieuwenhuys, B. E., *Surf. Sci.* **105**, 299 (1981).
82. Koerts, T., Welters, W. J. J., van Wolput, J. H. M. C., and van Santen, R. A., *Catt. Lett.* **16**, 287 (1992).
83. Mori, T., Masuda, H., Imai, H., Miyamoto, A., Baba, S., and Murakami, Y., *J. Phys. Chem.* **86**, 2753 (1982).
84. Shustorovich, E., and Bell, A. T., *J. Catal.* **113**, 341 (1988).
85. Williams, K. J., Ph.D. thesis, Department of Chemical Engineering, University of California, Berkeley, 1991.
86. Yates, J. T., Worley, S. D., Duncan, T. M., and Vaughan, R. W., *J. Chem. Phys.* **70**, 1225 (1979).
87. Winslow, P., and Bell, A. T., *J. Catal.* **94**, 385 (1985).
88. Mochida, I., Ikeyama, N., Ishibashi, H., and Fujitsu, H., *J. Catal.* **110**, 159 (1988).